7-2012

Sensitivity of Circumpolar Deep Water Transport and Ice Shelf Basal Melt along the West Antarctic Peninsula to Changes in the Winds

Michael S. Dinniman
Old Dominion University, msd@ccpo.odu.edu

John M. Klinck
Old Dominion University, jklinck@odu.edu

Eileen E. Hofmann
Old Dominion University, ehofmann@odu.edu

Follow this and additional works at: https://digitalcommons.odu.edu/ccpo_pubs

Part of the Oceanography and Atmospheric Sciences and Meteorology Commons

Repository Citation

Original Publication Citation

Sensitivity of Circumpolar Deep Water Transport and Ice Shelf Basal Melt along the West Antarctic Peninsula to Changes in the Winds

MICHAEL S. DINNIMAN, JOHN M. KLINCK, AND EILEEN E. HOFMANN

Center for Coastal Physical Oceanography, Old Dominion University, Norfolk, Virginia

ABSTRACT

Circumpolar Deep Water (CDW) can be found near the continental shelf break around most of Antarctica. Advection of this relatively warm water (up to 2°C) across the continental shelf to the base of floating ice shelves is thought to be a critical source of heat for basal melting in some locations. A high-resolution (4 km) regional ocean–sea ice–ice shelf model of the west Antarctic Peninsula (WAP) coastal ocean was used to examine the effects of changes in the winds on across-shelf CDW transport and ice shelf basal melt. Increases and decreases in the strength of the wind fields were simulated by scaling the present-day winds by a constant factor. Additional simulations considered effects of increased Antarctic Circumpolar Current (ACC) transport. Increased wind strength and ACC transport increased the amount of CDW transported onto the WAP continental shelf but did not necessarily increase CDW flux underneath the nearby ice shelves. The basal melt underneath some of the deeper ice shelves actually decreased with increased wind strength. Increased mixing over the WAP shelf due to stronger winds removed more heat from the deeper shelf waters than the additional heat gained from increased CDW volume transport. The simulation results suggest that the effect on the WAP ice shelves of the projected strengthening of the polar westerlies is not a simple matter of increased winds causing increased (or decreased) basal melt. A simple budget calculation indicated that iron associated with increased vertical mixing of CDW could significantly affect biological productivity of this region.

1. Introduction

Circumpolar Deep Water (CDW), which is derived from a mixture of the deep waters from all the world's oceans (Orsi et al. 1995), is the largest water mass by volume transported by the Antarctic Circumpolar Current (ACC). This water mass, characterized by temperature above 0°C and salinity greater than 34.6, is typically divided into upper Circumpolar Deep Water (UCDW), which rises to 200 m at its southern boundary and is distinguished by low oxygen ($O_2 < 4.5$ mL L^{-1}) (Sievers and Nowlin 1984) and high nutrient concentrations, and lower Circumpolar Deep Water (LCDW), which is distinguished by higher salinity (>34.7) (Orsi et al. 1995). These differences are due to the source regions of these water masses (Callahan 1972; Whitworth and Nowlin 1987).

The southern terminus of UCDW is used to define the poleward boundary of the ACC (Orsi et al. 1995). In most of the Amundsen–Bellingshausen Sea region (Fig. 1), this boundary abuts the continental shelf break (Orsi et al. 1995). Intrusions of CDW onto the continental shelf are observed at several locations where the ACC encounters irregular bathymetry (Klinck et al. 2004; Walker et al. 2007; Martinson et al. 2008; Moffat et al. 2009; Wåhlin et al. 2010). These intrusions flood the shelf below the permanent pycnocline and may be caused by momentum advection forcing flow across the shelf break because of the curvature of the bathymetry (Dinniman and Klinck 2004). The observed frequency (4 events per month) and duration (typically 1–3 days) of UCDW intrusions (Moffat et al. 2009) on the western Antarctic Peninsula (WAP) shelf suggest that the winds are an important component of the dynamics that move the CDW onto the continental shelf. Modeling studies in the Amundsen (Thoma et al. 2008) and Bellingshausen (Dinniman et al. 2011) Seas have highlighted the importance of winds in the CDW intrusion process, although the exact mechanisms involved are unresolved.

Corresponding author address: Michael S. Dinniman, Center for Coastal Physical Oceanography, Old Dominion University, 4111 Monarch Way, Norfolk, VA 23508-2559.
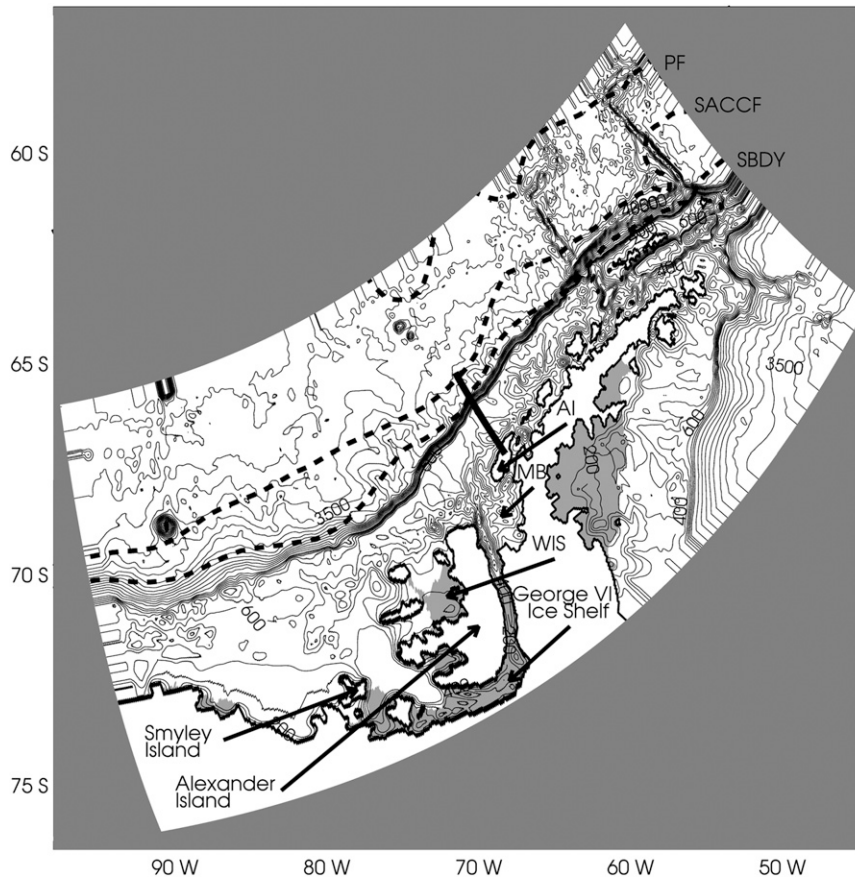E-mail: msd@ccpo.odu.edu

FIG. 1. Domain for the WAP model, showing bathymetry (100-m interval to 1000 m and 250-m interval deeper than 1000 m), ice shelves (shaded areas), and water column thickness below the ice shelves (e.g., average water column thickness below George VI Ice Shelf is 370 m). Dashed lines represent the climatological locations (from Orsi et al. 1995) of the polar front (PF—mostly north of the model domain), southern ACC front (SACCF), and southern boundary of the ACC (SBDY). Geographic names are abbreviated as Adelaide Island (AI), Marguerite Bay (MB), and Wilkins Ice Shelf (WIS). The line starting at Adelaide Island and extending off the continental shelf shows the extent of the cross sections shown in Figs. 4 and 7.

Intrusions of CDW extend to the inner continental shelf in many areas along the Amundsen coast (Jacobs et al. 1996) and WAP (Klinck et al. 2004). As a result, warm (relative to freezing) water is brought into contact with the base of the floating part of glaciers (ice shelves) that extend from the land out over the continental shelf ocean. Intrusions of CDW have been suggested as the primary mechanism that provides heat for basal melting of the Pine Island Glacier in the Amundsen Sea (Jacobs et al. 1996; Jenkins et al. 1997; Hellmer et al. 1998; Walker et al. 2007) and the George VI Ice Shelf (GVIIS) in the Bellingshausen Sea (Potter and Paren 1985; Talbot 1988; Jenkins and Jacobs 2008). The available evidence suggests that CDW presence is a component of basal melting of ice shelves, and changes in the frequency,

duration, and extent of cross-shelf intrusions of CDW may alter the rate at which this melting occurs.

The Southern Annular Mode (SAM), the principal mode of variability in the atmospheric circulation in the high southern latitudes (Thompson and Wallace 2000; Marshall 2003), has shifted toward positive polarity (decreased pressure over the Antarctic and increased pressure at midlatitudes) in recent years (Marshall 2003). The SAM trends appear to be driven both by increases in greenhouse gases and losses in stratospheric ozone (Shindell and Schmidt 2004) and some modeling studies suggest that the SAM trend will continue in this direction in the near future (Miller et al. 2006). However, there are indications that the expected disappearance of the ozone hole may have a stronger effect on the

SAM than projected further greenhouse gas increases leading to a reversal of the trend, at least in summer (Perlwitz et al. 2008; Son et al. 2008). Continued movement of the SAM toward positive polarity will result in strengthening and poleward displacement of the circumpolar westerlies. For the Antarctic Peninsula region, a positive SAM index has been related to warming (Kwok and Comiso 2002; Thompson and Solomon 2002; Van den Broeke and van Lipzig 2003), strengthening of the westerlies, especially during summer (Marshall et al. 2006), and increased frequency of mesoscale cyclones and a shift in storm tracks to favor more eastbound trajectories (Lubin et al. 2008). A positive SAM has also been linked to decreases in the sea ice extent and seasonal duration in the Antarctic Peninsula area (Lefebvre et al. 2004; Liu et al. 2004; Stammerjohn et al. 2008b).

It has been speculated that the stronger westerlies associated with a positive SAM will result in more CDW moving onto the Antarctic continental shelf, leading to an increased transport of heat and perhaps increasing the melting beneath ice shelves (Jacobs 2006). These changes in the winds may also lead to more vertical mixing and loss of this heat to the atmosphere. However, if the intruded waters move under the ice shelves quickly enough to retain most of the excess heat, then an increased rate of basal melting could occur. Also, strengthening of the westerlies may not necessarily increase the net transport of the ACC, but instead lead to increased eddy activity (Meredith and Hogg 2006; Hogg et al. 2008), which could also increase the transport of CDW onto the continental shelf in locations where the ACC is close to the shelf break.

The primary objective of this study is to examine the sensitivity of transport of CDW onto the WAP continental shelf and to the base of the GVIIS and Wilkins Ice Shelf (WIS) (Fig. 1) to changes in the winds and the ACC. This study also examined the effect of the changes in the CDW on the basal melt beneath GVIIS and WIS and the effects of changes in the winds and ACC transport on sea ice extent and transport of micronutrients into the euphotic zone. This process-oriented study used a regional circulation model that was configured for the Bellingshausen Sea/WAP region (Dinniman et al. 2011). Simulations forced by winds scaled by a constant (stronger or weaker) factor and with an increased ACC transport were used to address the study objectives. Other than the cases where the ACC is changed, possible global- or circumpolar-scale ocean effects (such as increases in the bulk temperature of the CDW, changes in temperature or salinity of other off-shelf water masses, and changes in ice concentration advected into the domain) were not considered.

2. Circulation model and experiments

a. Model structure

The Bellingshausen Sea–WAP model uses the Regional Ocean Modeling System (ROMS), which is a primitive equation, finite difference model with a terrain-following vertical coordinate system (Haidvogel et al. 2008; Shchepetkin and McWilliams 2009). The model domain extends from the Bellingshausen Sea near Thurston Island in the west, along the western side of the Antarctic Peninsula and into the Scotia Sea (Fig. 1). The model resolution is 4 km in both horizontal dimensions and includes 24 vertical levels, which vary in thickness with the water column depth but are concentrated toward the top and bottom surfaces. The model bathymetry (bedrock depth and draft below mean sea level of any floating ice shelves) was specified from sources that include 2-minute gridded elevations–bathymetry for the world (ETOPO2v2; Smith and Sandwell 1997), BEDMAP gridded data (Lythe et al. 2001), a gridded high-resolution bathymetry for the Marguerite Bay area of the WAP (Bolmer 2008), and measurements of the ice shelf thickness and bed elevation in the GVIIS area (Maslanyj 1987). Portions of the WIS collapsed in 2008 and 2009 (Scambos et al. 2009; Humbert et al. 2010). However, the base simulation was developed for 1 January 2000–31 December 2002 [to link to the Southern Ocean Global Ocean Ecosystems Dynamics Program field measurements (Hofmann et al. 2002)], which predates the collapse and the bathymetry reflects the pre-collapse ice shelf extent.

A dynamic sea ice model (Budgell 2005) was coupled to the circulation model to prognostically calculate ice concentration and thickness. The sea ice model is based on ice thermodynamics described by Mellor and Kantha (1989) and Häkkinen and Mellor (1992). A snow layer is included, which acts as an insulating layer and changes the surface albedo. A simple estimate of frazil ice production is also included (Steele et al. 1989). Ice dynamics are based on an elastic–viscous–plastic rheology (Hunke and Dukowicz 1997; Hunke 2001). This model also includes the mechanical and thermodynamic effects of ice shelves on the waters beneath as described in Dinniman et al. (2007) except that the heat and salt transfer coefficients are no longer constant but are functions of the friction velocity (Holland and Jenkins 1999). Additional details of the model configuration are given in Dinniman et al. (2011).

b. Initial and boundary conditions

Initial distributions of temperature and salinity were computed from the Simple Ocean Data Assimilation (SODA version 1.4.2) ocean reanalysis (Carton and

Giese 2008), and initial fields of ice concentration were obtained from Special Sensor Microwave Imager (SSM/I) satellite observations. Open boundaries for the base simulation were handled as in Dinniman and Klinck (2004), except that the temperature, salinity, and depth-averaged velocity for the boundaries were specified as monthly climatologies derived from the SODA reanalysis and ice concentration (from SSM/I) is now needed on the boundaries. Ice thickness in the initial and boundary conditions was set to 0.5 m. Most of the atmospheric conditions needed to force the coupled circulation–sea ice model (e.g., air temperature, humidity, sea level pressure, and precipitation) were taken from a monthly climatology derived from forecasts from the Antarctic Mesoscale Prediction System (AMPS; Powers et al. 2003; Bromwich et al. 2005), which uses a mesoscale meteorological model to compute high-resolution atmospheric forecast fields for operational use in Antarctica. The model-derived atmospheric fields were obtained at 30-km horizontal spacing at 12-h intervals. The winds used in the simulations are described in section 2c. Open ocean momentum, heat, and freshwater (imposed as a salt flux) fluxes for the model were calculated based on the Coupled Ocean–Atmosphere Response Experiment (COARE) 3.0 bulk flux algorithm (Fairall et al. 2003) and there was no relaxation of surface temperature or salinity to climatology. Tidal forcing was not included in the model.

c. Wind forcing and ACC transport

The AMPS 30-km model domain provided full coverage of the WAP model domain only after November 2002, which is after the period chosen for the base simulation. Therefore, wind forcing was taken from 6-hourly winds, distributed on a ½° grid, obtained from a blend of Quick Scatterometer (QuikSCAT) data and National Centers for Environmental Prediction (NCEP) analyses (Milliff et al. 2004). Changes in the mean westerlies and the strength of mesoscale cyclones were imposed by scaling each component of the QuikSCAT–NCEP blended winds by a constant factor. The base simulation used the unscaled winds, and simulations that tested the effects of decreased and increased wind speed were done by scaling each component of the wind by 0.8, 1.2, and 1.5 (Table 1). A 50% increase in wind strength is likely not realistic, but observations at the northern tip of the Antarctic Peninsula show that the mean westerly flow, which is not the same as the mean scalar wind speed, at a height of 850 hPa increased from 7 to 12.5 m s^{-1} from 1969 to 1998 (Marshall et al. 2006). The constant scaling factor maintains the structure of the winds (changes in divergence and curl are spatially uniform) while only changing their magnitude.

TABLE 1. Summary of model simulations. The current winds are the blended QuikSCAT–NCEP winds for the years 2000–02. Modifications to the current wind fields consisted of scaling each wind component by a constant factor that decreased the wind strength by 20% (0.8), or increased it by 20% (1.2) or 50% (1.5). The SACCF gradient was modified from current conditions by sharpening the density structure and inclusion of this in a simulation is designated by +. The vertical mixing schemes used in the simulations (see text) were a modified K-profile parameterization (KPP) scheme (KPP + mod), the standard KPP scheme (Basic KPP), and MY 2.5. Two of the highest wind simulations (1.5 and 1.5K) did not run to completion because of difficulties with specific extreme events.

Simulation	Wind strength	SACCF gradient	Vertical mixing scheme
Base	Current	Current	KPP + mod
Base+	Current	Sharpened	KPP + mod
0.8	Current × 0.8	Current	KPP + mod
1.2	Current × 1.2	Current	KPP + mod
1.2+	Current × 1.2	Sharpened	KPP + mod
1.5	Current × 1.5	Current	KPP + mod
BaseK	Current	Current	Basic KPP
BaseK+	Current	Sharpened	Basic KPP
0.8K	Current × 0.8	Current	Basic KPP
1.2K	Current × 1.2	Current	Basic KPP
1.2K+	Current × 1.2	Sharpened	Basic KPP
1.5K	Current × 1.5	Current	Basic KPP
BaseM	Current	Current	MY 2.5
BaseM+	Current	Sharpened	MY 2.5
0.8M	Current × 0.8	Current	MY 2.5
1.2M	Current × 1.2	Current	MY 2.5
1.2M+	Current × 1.2	Sharpened	MY 2.5
1.5M	Current × 1.5	Current	MY 2.5

The dynamical balance that describes the transport of the ACC in a given location is still a subject of study (Gnanadesikan and Hallberg 2000; Olbers et al. 2004), but it is clearly influenced by global forcings. The ACC transport was externally imposed in the WAP model by relaxing the temperature and salinity to the SODA data climatology over the 10 grid points closest to the lateral open boundary using the flow relaxation scheme of Martinsen and Engedahl (1987). The 0.25° × 0.4° horizontal resolution of these data and the temporal averaging provides a smoothed representation of the meandering ACC fronts. Two ACC fronts, the Southern ACC Front (SACCF) and the Polar Front (PF), are present in the model domain (Fig. 1), although the PF only goes through the northern corner of the domain.

Increased transport of the ACC was simulated by strengthening the SACCF in the imposed SODA data using a feature model approach (e.g., Fach and Klinck 2006) in which a front is defined by an anomaly which is added to the boundary data at the locations where the SACCF front appears in the SODA data. For this study, the SACCF was modified by a salinity anomaly; no change was made to the temperature.

The enhanced salinity front was defined by a salinity anomaly (S_a) that decayed with depth (z) and horizontal distance from the front location (y_r, positive seaward from the front) as

$$S_a = \Delta S y_r \exp[-(y_r/2W)^2] \exp(z/Z_d) \min\left(1, \frac{-z}{Z_s}\right), \quad (1)$$

where ΔS is the salinity change across the front, set to be -0.12 psu $(100 \text{ km})^{-1}$, W and Z_d are the width (30 km, Fach and Klinck 2006) and depth (1200 m, Fach and Klinck 2006) scales of the front, respectively, and Z_s is the surface layer depth (300 m) defined for the front. The minimum function prevents the frontal structure from intruding into the surface mixed layer. The salinity change across the front was increased slightly from the estimated observed value of -0.09 psu $(100 \text{ km})^{-1}$ (Fach and Klinck 2006) for the sharpened SACCF experiments to force an increased ACC transport relative to current conditions. The average total model transport along the SACCF across an 80-km section of the front halfway between the western and eastern open boundaries was 16.0 Sv (1 Sv $\equiv 10^6$ m^3 s^{-1}) for the base simulation, which compares well with an estimate of 15 Sv for the baroclinic transport over an 80-km section across the SACCF at 85°W (Read et al. 1995). Two simulations were run with a sharpened SACCF (Table 1) and the total model transport along the SACCF with the base winds increased to 16.8 Sv, which is about the same as the SACCF transport (16.9 Sv) for the case with a 20% increase in the wind strength.

d. Simulation implementation

The WAP model was initialized in mid-September and run for slightly over four years with a two-year repeating cycle of daily winds (from AMPS) and monthly climatologies for all other forcing. All the model simulations presented here begin from the same spinup state. At the end of this model spinup, dye representing CDW, defined by temperature greater than 0.0°C below 200 m, was placed off the continental shelf (no dye was initialized on the shelf) with an initial concentration of 100. The simulation was continued from 1 January 2000 through 31 December 2002 and the CDW dye was allowed to advect and diffuse over the model domain. Throughout the simulation there was a continuous source of dye into the model domain from the off-shelf CDW because the boundary conditions also contained dye. There was no surface or bottom vertical flux of dye and there were no sinks of dye other than advection out of the model domain at the open boundaries.

Vertical momentum and tracer mixing were computed using the K-profile parameterization (KPP; Large

et al. 1994) mixing scheme implemented in ROMS with a modification (Dinniman et al. 2011). The surface boundary layer depth under stabilizing conditions with non-zero surface shortwave flux was set to a minimum depth, equal to the directly wind forced minimum depth under stable conditions in a Kraus–Turner bulk mixed layer model (Niiler and Kraus 1977; Dinniman et al. 2003). The unmodified KPP scheme may have difficulties with a dynamic sea ice model implemented over Antarctic continental shelves (Timmermann and Beckmann 2004), and the approach used in this study provided the best representation of the seasonal vertical mixing in the WAP region (Dinniman and Klinck 2004; Dinniman et al. 2011). However, because vertical mixing is critical in understanding the effects of modified winds and ACC transport, simulations were also done (Table 1) using the unmodified KPP and the Mellor–Yamada 2.5 (MY2.5) schemes (Mellor and Yamada 1982).

3. Results

a. Simulation of current state

Evaluation of the simulated transport of CDW onto the WAP continental shelf and underneath GVIIS and the seasonal cycle of vertical temperature structure on the continental shelf is given in Dinniman et al. (2011). The simulated pathways of CDW onto the continental shelf were shown to match observations. Animations of the simulated dye concentrations [see supplemental material to Dinniman et al. (2011) online at http://www.ccpo.odu.edu/~msd/DSRpaper/WAP_animation.gif] show the time evolution of CDW intrusions onto the WAP shelf, flooding of the shelf below the pycnocline by this water mass, and penetration of CDW into the inner shelf, including the areas around the entrances to the cavities beneath GVIIS and WIS.

The annual average basal melt rate of the GVIIS obtained from the base simulation was 5.8 m yr^{-1}. This rate is similar to that obtained by Dinniman et al. (2011), 6.0 m yr^{-1}, from a simulation that used different winds, but greater than estimates derived from observations of 2.1 m yr^{-1} (Potter and Paren 1985), 2.8 m yr^{-1} (Corr et al. 2002), and 3.1–4.8 m yr^{-1} (Jenkins and Jacobs 2008).

The annual average basal melt rate of the WIS in the base simulation was 0.5 m yr^{-1}. Padman et al. (2012) estimate that the mean basal melt of WIS was 1.7–2.3 m yr^{-1} over the period 1992–2000 and was 0.3–0.9 m yr^{-1} for 2001–2008. The bathymetry (ice thickness and bed elevation) around and underneath WIS is poorly known (Padman et al. 2010) and this will contribute to model errors in estimating the basal melt. Holland et al. (2010) used the same WIS thickness as used in this
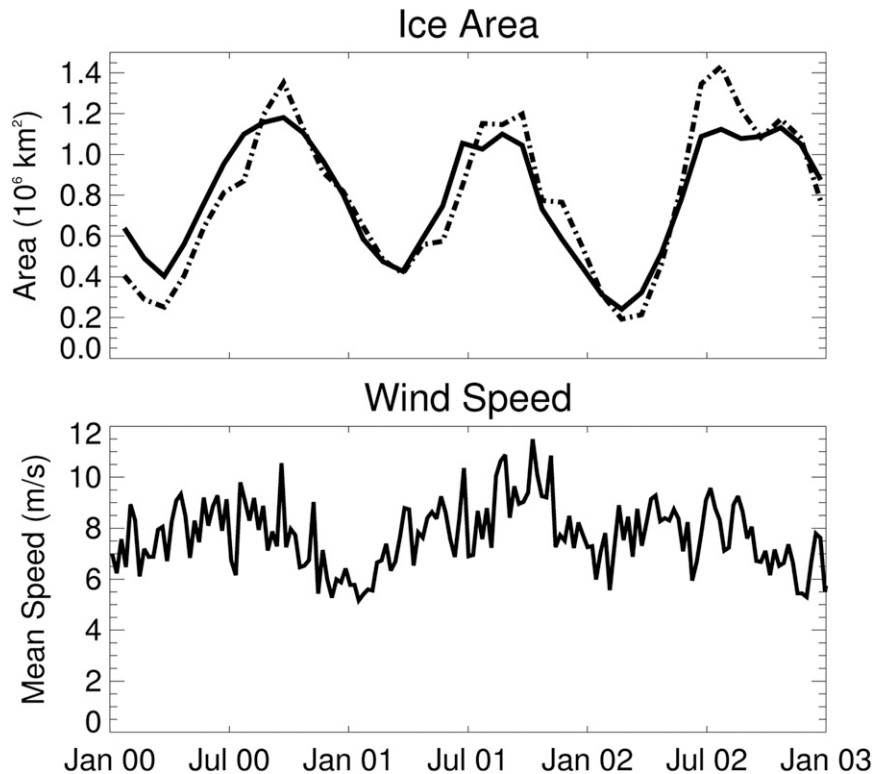
FIG. 2. (top) Monthly simulated (solid line) and observed SSM/I (dotted) sea ice area (10^6 km^2) calculated for the entire model domain. (bottom) Weekly mean QuikSCAT–NCEP wind speed (m s^{-1}) averaged over the entire model domain.

study and obtained a similar value (0.7 m yr^{-1}) for the melt rate beneath WIS.

The skill in simulating sea ice was assessed by interpolating SSM/I monthly ice concentrations onto the model grid and calculating the total sea ice area (sum of the sea ice concentration in one grid cell x grid cell area) over different parts of the model domain. The SSM/I-derived monthly average areas were compared to estimates obtained from the simulated sea ice distributions. A comparison (Fig. 2) over the entire model domain showed that the simulated sea ice distribution in the base case (Table 1) accurately captured the primary seasonal response ($r = 0.935$). The skill in simulating the ice extent was also assessed using the Willmott (1981) index of agreement, which was developed to overcome the insensitivity of correlations to differences in observed and model-simulated means and variances, and is given as

$$\text{Skill} = 1 - \left[\sum_{i=1}^{N} (X_{\text{sim}} - X_{\text{obs}})^2 \bigg/ \sum_{i=1}^{N} (|X_{\text{sim}} - \overline{X_{\text{obs}}}| + |X_{\text{obs}} - \overline{X_{\text{obs}}}|)^2 \right], \quad (2)$$

where the simulated and observed values are given by X_{sim} and X_{obs}, respectively. A skill value of 0.0 represents complete disagreement and 1.0 represents perfect agreement. Over the entire model domain, the model skill obtained using Eq. (2) was 0.956. Removal of the average seasonal cycle still resulted in model skill ($r = 0.622$, skill = 0.765) in simulating the interannual anomalies in the total ice area. Note that SSM/I-based ice concentrations are used as a bottom boundary condition for both the AMPS and NCEP models. Thus, the atmospheric forcing should force the ocean model toward these observations. Evaluation of model skill in simulating the total ice area over the portion of the continental shelf that extends from Smyley Island to the northern tip of Adelaide Island (Fig. 1), which is the WAP shelf area in front of the entrances to the WIS and GVIIS cavities, showed reasonable representation of the seasonal response (not shown, $r = 0.848$, skill = 0.916), but less skill in predicting the interannual anomalies after removal of the local seasonal mean ($r = 0.397$, skill = 0.614). Some of this reduced skill in simulating the local interannual anomalies was due to a failure to capture the late sea ice retreat in spring–summer 2001/2002 in this area, which could be a result of difficulties in simulating
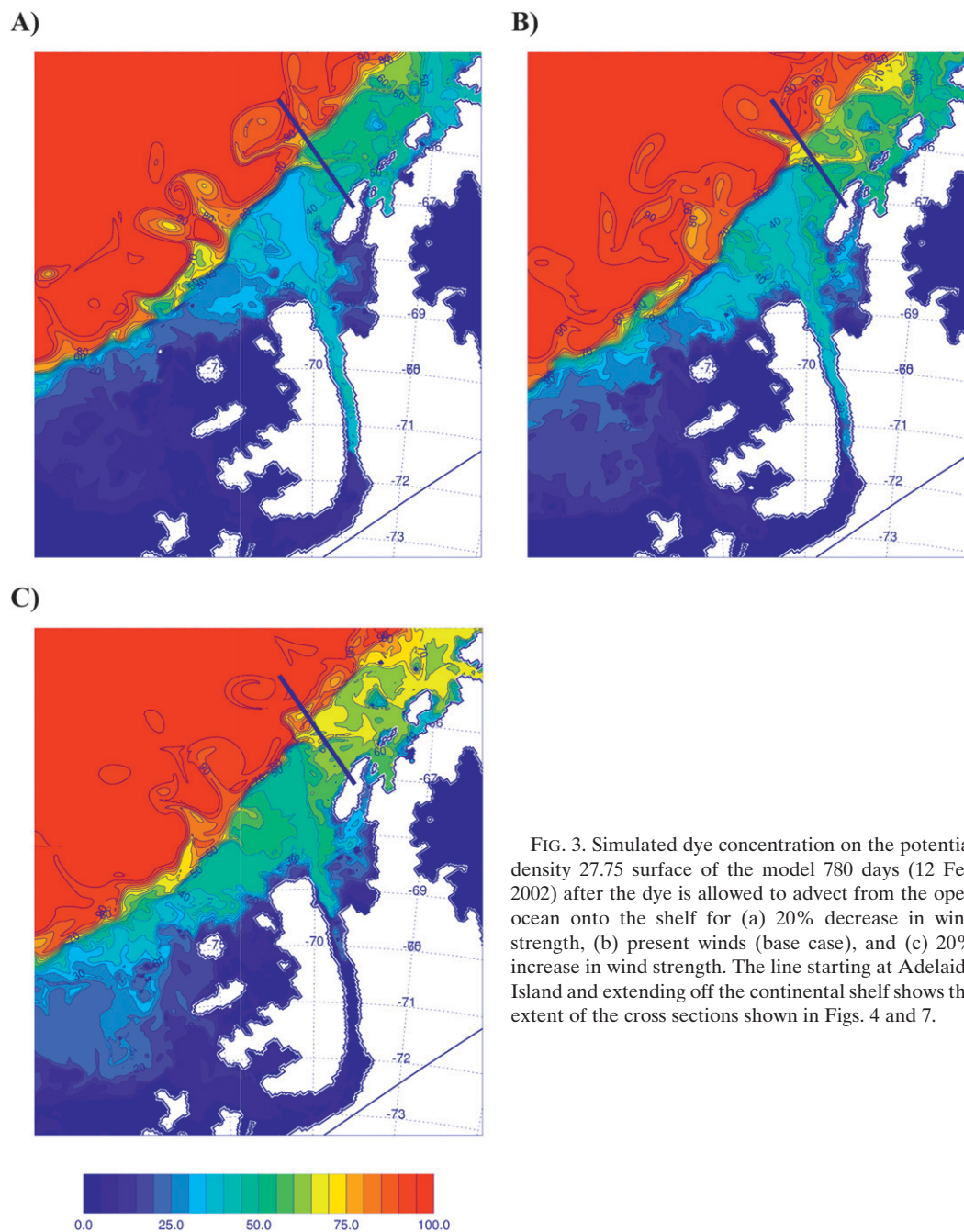
A)

B)

C)

FIG. 3. Simulated dye concentration on the potential density 27.75 surface of the model 780 days (12 Feb 2002) after the dye is allowed to advect from the open ocean onto the shelf for (a) 20% decrease in wind strength, (b) present winds (base case), and (c) 20% increase in wind strength. The line starting at Adelaide Island and extending off the continental shelf shows the extent of the cross sections shown in Figs. 4 and 7.

the extremely thick ice (10–20 m) along the coast that year due to anomalously strong north–northwesterly winds (Massom et al. 2006).

b. Changes in CDW and vertical temperature distribution

The amount of CDW dye transported onto the WAP continental shelf depended on the wind strength. Comparison of the dye concentrations on the shelf from simulations in which the winds were increased and decreased by 20% relative to the base simulation (Fig. 3) showed that stronger winds moved more CDW onto the open shelf almost everywhere. The dye concentration along an across-shelf vertical section near Adelaide Island (Fig. 4) showed more dye on the continental shelf and more mixing upward into surface waters (both on and off the shelf) with increased winds. The water column mean dye concentration (Fig. 5) for the portions of
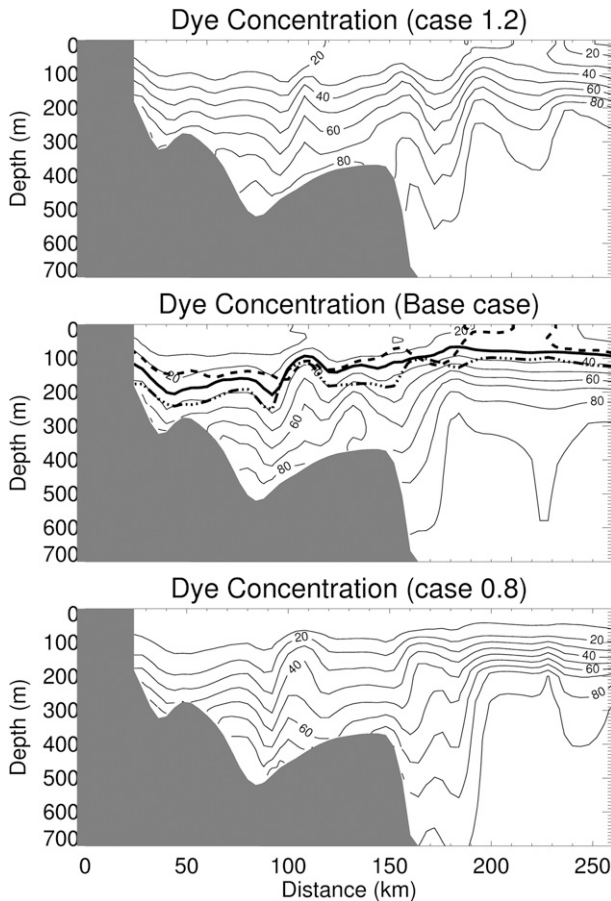
FIG. 4. Simulated vertical distribution of dye concentration along the section off Adelaide Island (Fig. 1) 780 days (12 Feb 2002) after the dye is allowed to advect from the open ocean onto the shelf for a (top) 20% increase in wind strength, (middle) present winds (base case), and (bottom) 20% decrease in wind strength. The heavy solid line in the base case plot is the 30 dye unit contour, the dashed line is the 30 dye unit contour from case 1.2, and the dashed-dot line is the 30 dye unit contour from case 0.8. The gray shading represents land.

the continental shelf between Smyley Island and the north end of Adelaide Island that are not underneath an ice shelf showed that the quantity of CDW on the shelf increased as the winds increased. The amount of CDW on the shelf also increased with stronger ACC transport.

The amount of CDW dye that moved underneath GVIIS did not necessarily increase with increasing wind strength. Increasing the wind strength by 50% produced the highest dye concentration underneath GVIIS (Fig. 6). However, the weakest winds (reduction by 20%) produced the second highest dye concentration and slightly increased winds (20%) resulted in less CDW dye underneath GVIIS, relative to the base simulation. Increasing the ACC transport had only a small effect on the dye concentration underneath GVIIS. In contrast, increasing the winds and the ACC transport did increase
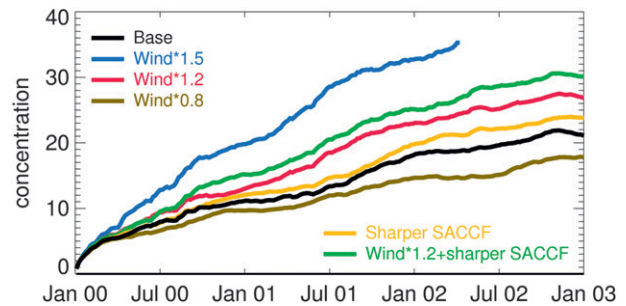

FIG. 5. Simulated mean dye concentrations obtained for the open portion of the WAP continental shelf from Smyley Island to the northern end of Alexander Island.

the amount of CDW dye underneath WIS (not shown) similar to the open continental shelf (Fig. 5), with the winds having a significant impact.

The vertical distribution of the simulated temperature in February along a section that extends from Adelaide Island across the WAP shelf showed that increasing the winds by 20% deepened the summer mixed layer and eroded and warmed (from above and below) the remnant cool winter water layer below the surface layer over the middle and outer continental shelf leading to a layer of warming over most of the shelf below the surface centered around 80 m (Fig. 7). The temperature was also warmer at depth right at the shelf break, but was cooler at depth over most of the shelf. Decreasing the winds by 20% led to a shallower summer mixed layer (especially near the coast) resulting in a thin layer of cooling below the surface over most of the shelf (Fig. 7). The water at depth over the outer shelf was slightly cooler, but the inner shelf water at depth was warmer. The horizontal location off the shelf break of the core of the warmest water is quite variable and moved back and forth in all cases. Winter conditions along the same section (not shown) showed that as the winds increased, a deeper cold surface mixed layer, deeper thermocline, and cooler temperatures at depth developed over the shelf.
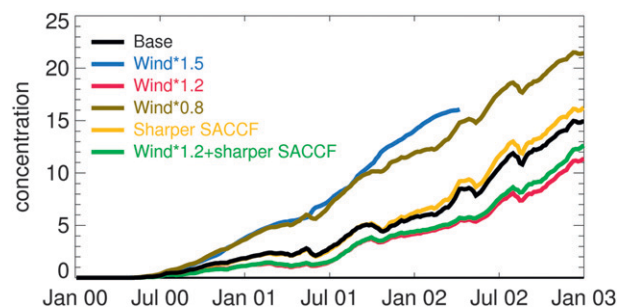

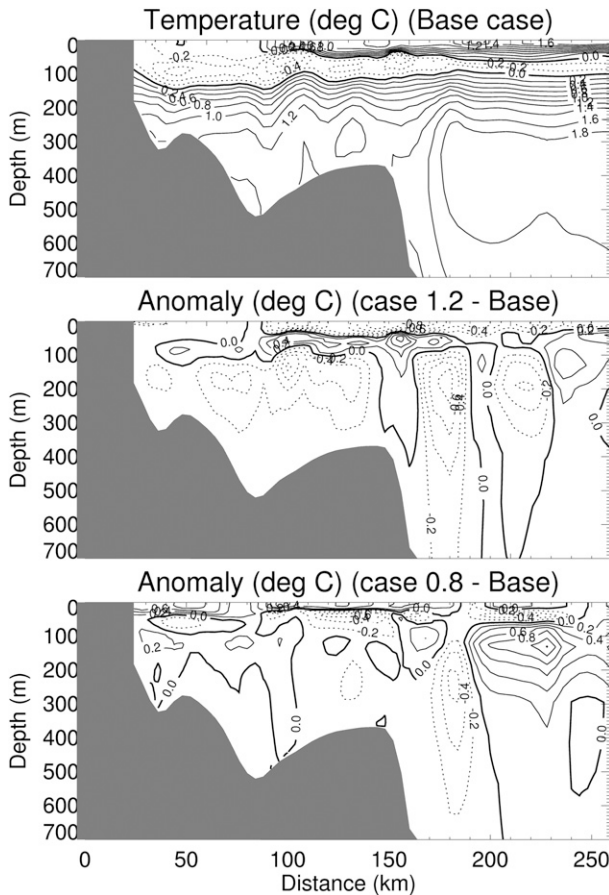FIG. 6. Simulated mean dye concentrations beneath George VI Ice Shelf.

FIG. 7. (top) Simulated vertical distribution of temperature along the section off Adelaide Island (Fig. 1) on 12 Feb 2002 for the base case. (middle) Temperature anomaly between a simulation with a 20% increase in wind strength and the base case above. (bottom) Temperature anomaly between a simulation with a 20% decrease in wind strength and base case at the top. Contour interval in all three panels is 0.2°C.
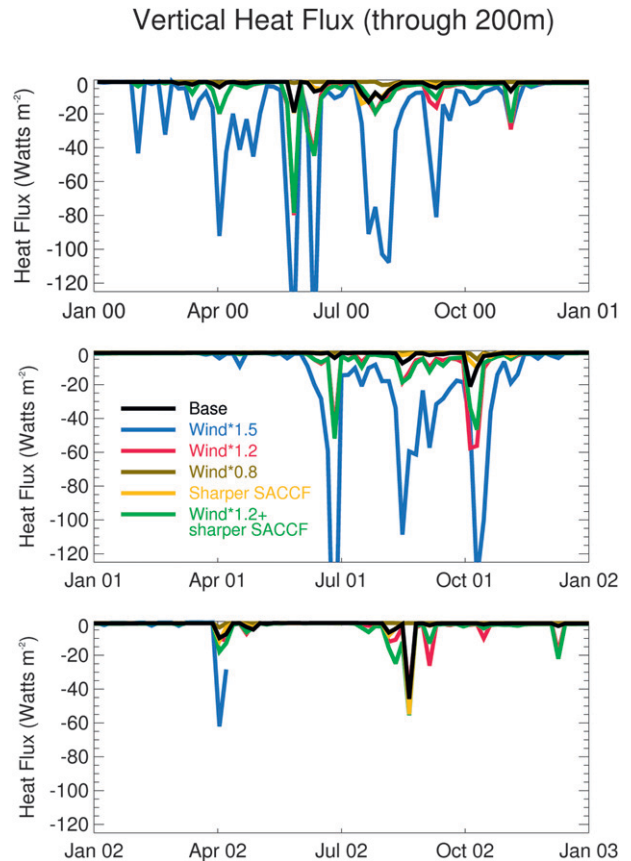

FIG. 8. Simulated vertical diffusive heat fluxes (vertical mixing) through 200 m for the open ocean portion of the WAP continental shelf from Smyley Island to the northern end of Adelaide Island for (top to bottom) January 2000–December 2002.

A comparison of the heat budgets for water below 200 m on the open areas of the WAP shelf from Smyley Island to just north of Adelaide Island showed that the vertical mixing term was strongly time variable (Fig. 8), especially with the stronger winds where the variability was often in response to significant wind events and was always negative (loss of heat to the waters above) with significantly more heat lost to the upper water when the winds are stronger (Table 2). Differences in the heat loss among the simulations with similar wind forcing but different ACC strength resulted from short-term episodic events. However, in the mean there was little difference in heat loss because of an accelerated ACC along the shelf break. The base case mean vertical mixing of -2.2 W m^{-2} through 200 m was within the range of estimates (1–5 W m^{-2}) from observations of the heat lost

from UCDW through the pycnocline (Klinck 1998; Smith and Klinck 2002; Howard et al. 2004).

c. Changes in ice shelf basal melt rate

The basal melt underneath GVIIS showed a response to wind strength that was opposite that of the CDW dye concentration on the open shelf. Basal melt rate decreased as the winds increased (Table 3; Fig. 9). Increasing the ACC transport had almost no effect on the basal melt rate. The basal melt rate did not show a seasonal cycle in any of the simulations, although some interannual variability, beyond the initial transient to a quasi-steady state, was apparent in the simulations. As found in Holland et al. (2010), there was much more interannual variability in the basal melt for the southern half of GVIIS than the northern half for the base case (not shown), but the change in the basal melt with different winds was similar in both halves (although a bit more pronounced in the south). The basal melt rate underneath WIS showed a different response to increased

TABLE 2. Summary of simulated mean vertical diffusive heat fluxes (W m^{-2}) through 200 m obtained from the different simulations for the region of the WAP continental shelf from Smyley Island to the northern end of Adelaide Island. Note that the 1.5 and 1.5K simulations did not run to completion.

Simulation	Vertical diffusive heat flux (W m^{-2})
Base	−2.2
Base+	−2.1
0.8	−1.1
1.2	−4.9
1.2+	−5.0
1.5	−19.0 (not full period)
BaseK	−1.1
BaseK+	−1.1
0.8K	−1.1
1.2K	−1.4
1.2K+	−1.4
1.5K	−9.5 (not full period)
BaseM	−2.7
BaseM+	−2.6
0.8M	−2.5
1.2M	−3.4
1.2M+	−3.5
1.5M	−10.4

TABLE 3. Summary of simulated mean basal melt rates (m yr^{-1}) beneath George VI Ice Shelf and Wilkins Ice Shelf obtained from the different simulations. Note that the 1.5 and 1.5K simulations did not run to completion.

Simulation	GVIIS basal melt (m yr^{-1})	WIS basal melt (m yr^{-1})
Base	5.78	0.51
Base+	5.80	0.51
0.8	7.65	0.33
1.2	4.02	0.79
1.2+	4.01	0.78
1.5	3.24 (not full period)	1.98 (not full period)
BaseK	6.58	0.45
BaseK+	6.59	0.46
0.8K	8.08	0.33
1.2K	4.87	0.72
1.2K+	4.94	0.73
1.5K	4.21 (not full period)	2.23 (not full period)
BaseM	6.00	0.49
BaseM+	6.04	0.50
0.8M	7.90	0.37
1.2M	4.34	0.74
1.2M+	4.28	0.74
1.5M	2.89	1.52

winds, with the basal melt increasing as the winds increased (Table 3; Fig. 10). The basal melt under WIS had a pronounced seasonal signal with the majority of the basal melting occurring in late summer–early fall. Increasing the ACC transport also had almost no effect on the basal melt beneath the WIS.

d. Changes in sea ice concentration

Changes in the strength of the winds have a pronounced effect on the simulated sea ice area and extent. The sea ice concentration on the continental shelf was reduced with stronger winds relative to the base simulation. Estimates of the total sea ice area for the region from Smyley Island to the northern tip of Adelaide Island (Fig. 11) showed that the total simulated sea ice area decreased as the winds increased. The decrease was pronounced in late summer–early fall when the total sea ice is at a minimum (Fig. 12). Observations show that the sea ice extent in the WAP area has decreased in time and that this decrease is more pronounced in spring–summer–fall than in winter (Smith and Stammerjohn 2001; Zwally et al. 2002).

e. Effect of vertical mixing parameterization

The primary mixing scheme used in this study was a modification to the default KPP method implemented in ROMS. Simulations that used the unmodified KPP scheme and the Mellor–Yamada level 2.5 turbulence closure scheme (Mellor and Yamada 1982) were done for comparison (Table 1). For the base wind simulations,

changing the mixing scheme only made a small difference in the basal melt beneath GVIIS with the modified KPP mixing case having the lowest mean basal melt (5.8 m yr^{-1}), followed by the MY2.5 case (6.0 m yr^{-1}) and then the default KPP case (6.6 m yr^{-1}). Independent of mixing scheme, the strongest winds always resulted in the lowest mean basal melt rate beneath GVIIS with the melt increasing as the winds decreased (Table 3). Increased transport of the ACC had little effect on the basal melt rate. Increasing the winds increased the basal melt underneath WIS for all three mixing schemes (Table 3), with little effect from a stronger ACC.

f. Estimated iron budget

The simulations provide estimates of CDW flux into a given volume. These flux estimates can be used to estimate the primary production that can be supported by the flux of dissolved iron into the euphotic zone, assuming an initial dissolved iron concentration in CDW. For the base simulation, an initial iron concentration in CDW of 0.5 nanomolar (nM, where 1 nM = 10^{-6} mol m^{-3}) (Sedwick et al. 2011) and a C:Fe algal assimilation ratio of 450 000 mol mol^{-1} (Tagliabue and Arrigo 2005) produced an iron flux into the upper 100 m that can support primary production of <1 g(C) m^{-2} yr^{-1} for the open WAP shelf (Table 4) over the growing season (1 November – 28 February of the first year of the simulation). Assuming that the dissolved Fe that advects or diffuses into the upper 100 m during an entire year is bioavailable during the growing season, then the estimate
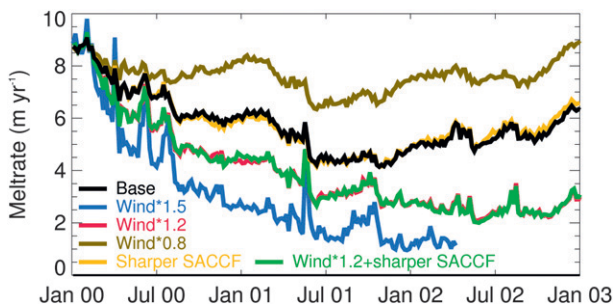
FIG. 9. Simulated mean basal melt rates underneath George VI
Ice Shelf.

FIG. 10. Simulated mean basal melt rates underneath Wilkins
Ice Shelf.

of enhanced CDW-supported productivity for the base
case increases to 10 g(C) m^{-2} yr^{-1}. The algal assimilation
ratio used here is not conservative (and probably only
appropriate for *Phaeocystis antarctica*), so this estimate
represents an upper bound. The estimated productivity
that can be supported by CDW intrusions increased with
stronger winds (Table 4). The estimates of WAP shelf
productivity, based on CDW flux over the entire year, in-
creased to 27 g(C) m^{-2} yr^{-1} for a 20% wind increase,
36 g(C) m^{-2} yr^{-1} for a 20% wind increase and enhanced
ACC transport, and 62 g(C) m^{-2} yr^{-1} for a 50% in-
crease in wind.

4. Discussion

a. CDW and ice shelf basal melt rate

Increased transport of CDW onto the Antarctic con-
tinental shelf as a result of increased wind strength has
been shown in previous modeling studies. Thoma et al.
(2008) showed that stronger westerly winds resulted in
larger inflows of CDW onto the continental shelf of
the Amundsen Sea. Dinniman et al. (2011) showed that
much of the timing of the CDW intrusions on the WAP
shelf was related to short period wind events, implying
that increased frequency and magnitude of such events
would increase the transport of CDW to the shelf. How-
ever, what seems counterintuitive is that the basal melt
rate underneath GVIIS decreased when the winds in-
creased and there was more CDW available on the ad-
jacent open shelf, especially since the basal melt rate
beneath WIS increased with stronger winds.

This result arises because, while the stronger winds
force more CDW onto the continental shelf, they also
enhance vertical mixing and the upward transport of
heat (Figs. 7 and 8). The mean depth below mean sea
level (MSL) of the base of GVIIS in the model ba-
thymetry is 245 m with a standard deviation of 96 m.
This places most of the ice shelf base in the model layer
that had a net heat loss over the WAP shelf with in-
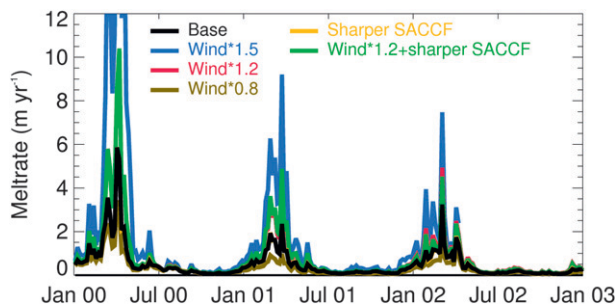creased wind strength. In the case of GVIIS, the winds

increased the CDW advected onto the shelf, but also
increased the mixing of this CDW at depth thereby re-
ducing the heat that was advected to the base of the ice
shelf. Holland et al. (2010) showed that the interannual
variability in the basal melt of GVIIS was controlled by
water mass transformations because of changes in sur-
face sea ice variability rather than by variations in the
cross-shelf transport of CDW. Thus, their conclusions
are compatible with those from this study because the
sea ice changes in their simulation are likely driven by
differences in the winds (e.g., their section 3.3). Both
studies show that variability in the winds over the con-
tinental shelf is the main driver of the variability in the
ice shelf basal melt.

The mean depth below MSL of the base of WIS in
the model bathymetry is about 70 m with a standard
deviation of 18 m. A more recent estimate of the mean
draft of WIS is 165 m with a range of 80–260 (Padman
et al. 2012). Padman et al. (2012) use temperatures de-
rived from instrumented seals to show that most of the
base of the WIS is within the winter water surrounding
WIS and is well above the core of the CDW and below
the summer surface layer. Even though the mean depths
differ substantially, both depth estimates place much of
the WIS base at a depth where increased CDW transport
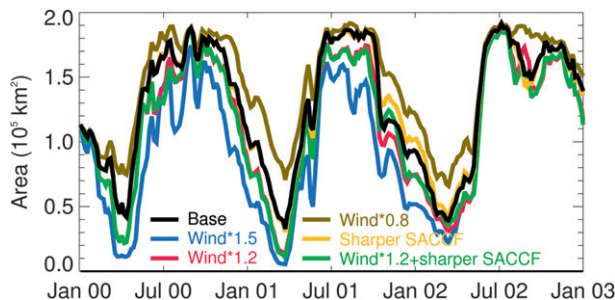onto the WAP shelf and increased loss of heat to upper

FIG. 11. Simulated monthly model sea ice areas calculated for the
region of the WAP continental shelf from Smyley Island to the
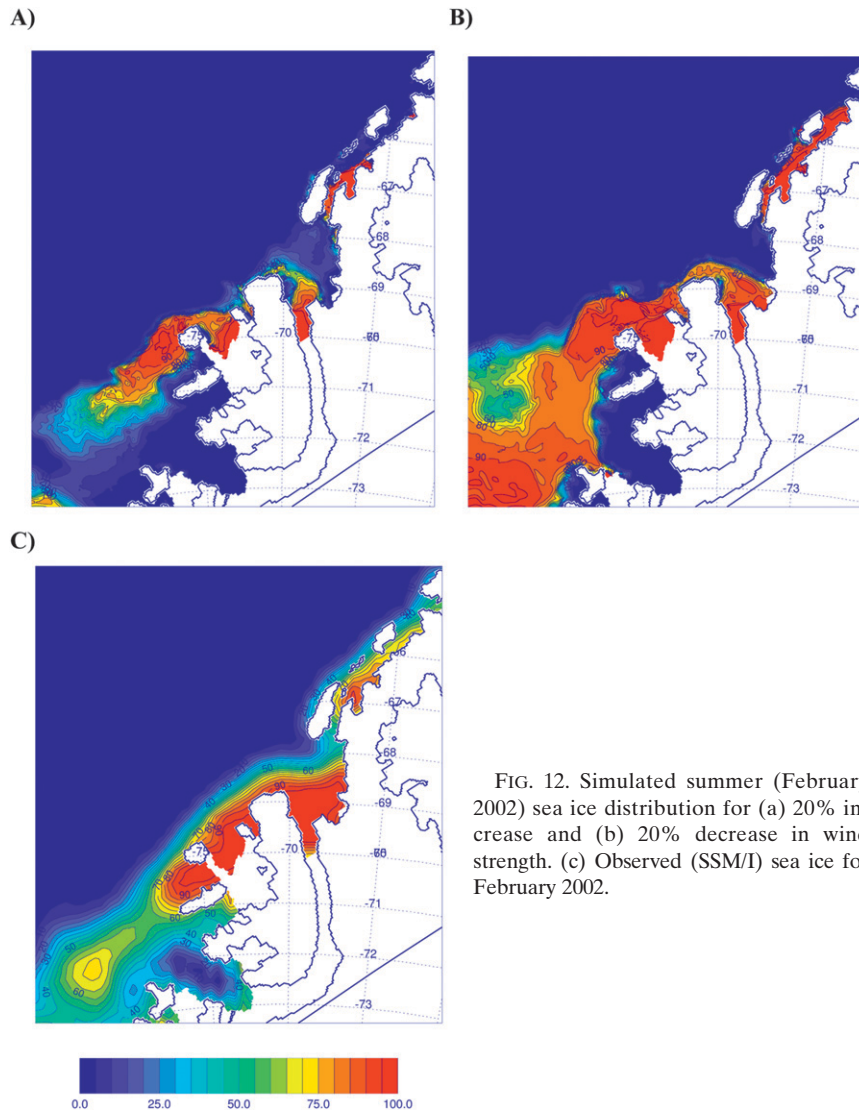northern end of Adelaide Island.

A)

B)

C)

FIG. 12. Simulated summer (February 2002) sea ice distribution for (a) 20% increase and (b) 20% decrease in wind strength. (c) Observed (SSM/I) sea ice for February 2002.

(but not necessarily surface) waters with increased winds result in heat gain at the base of the WIS, which enhances the basal melting.

The simulated basal melt rate of the WIS was strongly seasonally dependent with almost all melting occurring in the summer and fall (Fig. 10). Makinson et al. (2006) showed that along the Ronne Ice Shelf front in winter, when vertical stratification was weak, mean flows were along the ice shelf front. However, in summer, when the vertical stratification was strong, there was more baroclinicity in the near-ice-front currents, which allowed for more exchange of water into and out of the ice shelf cavity. The increased wind simulations showed reduced summer sea ice extent near the WIS. Whether the reduced summer sea ice is more a cause (due to winds moving ice and allowing for more solar insolation) or

a result (due to more vertical mixing) of more heat in the surface and near-surface waters near the WIS, either scenario allows warmer water to be transported underneath the WIS, producing the enhanced summer basal melt.

The relative magnitude of onshore CDW flux and vertical mixing on the shelf underlie the differences in the amount of CDW dye underneath WIS (not shown) and GVIIS (Fig. 6). For GVIIS, increasing the wind strength by 50% resulted in greatly increased flux of CDW onto the shelf, which compensated for increased mixing, resulting in a greater flux of CDW underneath GVIIS even though the total heat content (and basal melt) was less. Reducing the wind strength by 20% reduced vertical mixing enough to compensate for the lower on-shelf CDW flux, leading to increased CDW

TABLE 4. Estimated primary production [PP; g(C) m^{-2} yr^{-1}] that could be supported by the estimated flux of dissolved iron into the upper 100 m that is provided by CDW intrusions onto the WAP continental shelf. The PP estimates represent the iron flux over the growing season (1 November–28 February) and over the entire year from the first year of the simulation.

Simulation	PP – growing season [g(C) m^{-2} yr^{-1}]	PP – annual [g(C) m^{-2} yr^{-1}]
Base	0.5	10.5
Base+	0.7	12.1
0.8	0.0	3.7
1.2	4.9	27.4
1.2+	7.6	36.0
1.5	20.2	62.4
BaseK	3.2	13.8
BaseK+	2.2	12.0
0.8K	1.0	1.6
1.2K	6.5	27.8
1.2K+	8.0	27.5
1.5K	18.9	63.2
BaseM	6.0	18.9
BaseM+	2.7	14.1
0.8M	1.7	5.6
1.2M	9.2	31.0
1.2M+	9.1	33.4
1.5M	26.4	68.0

FIG. 13. Simulated average mass fluxes (cm day^{-1}, includes frazil ice production) between the sea ice and the ocean calculated for the region of the WAP continental shelf from Smyley Island to the northern end of Adelaide Island for (top to bottom) January 2000–December 2002.

flux underneath GVIIS and increased basal melt. Underneath WIS, a larger portion of the water cavity is above the depth at which CDW comes onto the shelf. Also, this ice shelf is closer to the shelf break, which reduces the exposure of CDW to wind mixing. Thus, vertical mixing is reduced and horizontal transport dominates the CDW supply for this ice shelf.

Once on the WAP shelf, the fate of the heat associated with CDW depends critically on the vertical mixing. Therefore, the vertical mixing parameterization used in the circulation model is of primary importance. However, increased winds always produced lower mean basal melt rates beneath GVIIS independent of the vertical mixing parameterization and vice versa (Table 3). Similarly, increased wind strength increased the basal melt underneath WIS for all three mixing schemes (Table 3). Increasing the transport of the ACC did not alter these results.

This study may have relevance to other areas of the Antarctic where CDW is present and potentially contributes to the basal melt of ice shelves. The west Antarctic Ice Sheet (WAIS) is thought to be losing volume because of outlet glaciers draining into the Amundsen Sea (Shepherd et al. 2002; Thomas et al. 2004; Pritchard et al. 2009) and the rate of loss has been increasing in recent years (Rignot et al. 2008; Chen et al. 2009). One proposed reason for the increased basal melt is a change in either the temperature or quantity of warm CDW that enters the subglacial area providing
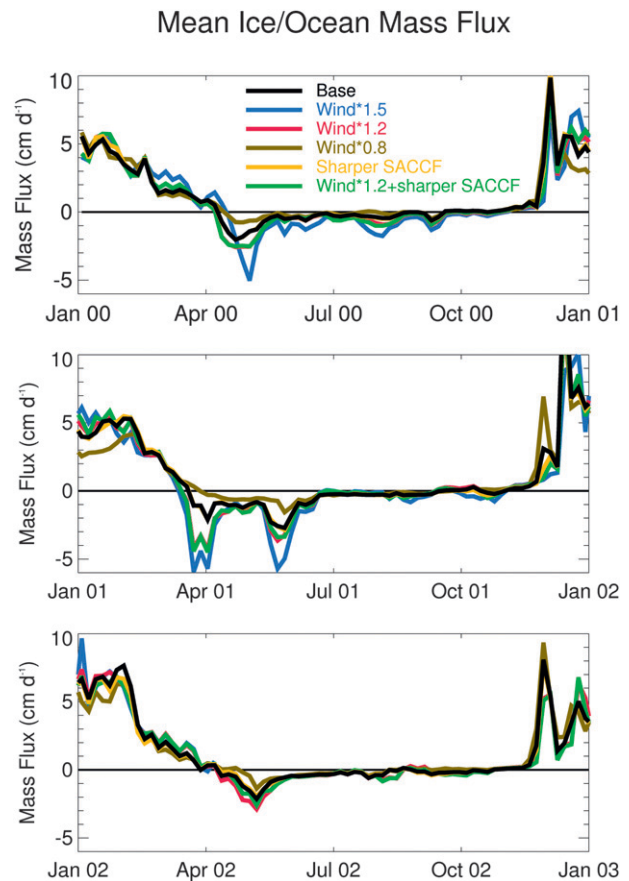
heat to increase the basal melt rate (Payne et al. 2004). In the Amundsen Sea, the glacier–outflow ice shelves, such as the tongue of Pine Island Glacier, have grounding lines that extend to the seabed, as opposed to the drafts of GVIIS and WIS that only extend partway through the water column (Holland et al. 2010). Also, the CDW tends to be deeper in the water column at the ice shelf front in the Amundsen Sea (Hellmer et al. 1998) than in front of GVIIS (Jenkins and Jacobs 2008), and therefore less affected by surface processes. Thus, ice shelves in the Bellingshausen–WAP region are likely to be more affected by changes in surface conditions than those along the Amundsen Sea, which may be more responsive to variability in the fluxes of CDW onto the continental shelf (Holland et al. 2010).

b. Sea ice

Observations have shown that strong decreases in the sea ice extent in the WAP area are often forced by

anomalously strong northerly winds, which reduce the extent of the ice by compacting it against the coast (Harangozo 2006; Massom et al. 2006, 2008; Stammerjohn et al. 2008a). Modeling studies have shown reductions in sea ice extent with increasing SAM (Lefebvre and Goosse 2005; Sen Gupta and England 2006) and that the reductions are due to both thermal effects from the atmosphere (increased surface air temperatures due to the stronger northerly winds) and mechanical effects (stronger advection of ice toward the continent). Increased mixed layer depth due to increased wind mixing also was a factor in reduction of sea ice extent (Lefebvre and Goosse 2005). The mean mass flux between the sea ice and ocean per unit ice area for the continental shelf between Smyley Island and the northern tip of Adelaide Island (Fig. 13) shows that some of the reduction in the simulated sea ice extent was driven by ocean thermodynamics and not just the result of mechanical wind drag compacting the ice against the coast. Generally the mass flux was more positive (ice melting into the ocean) with stronger winds during the summer and more negative (ocean water freezing into sea ice) with stronger winds during the winter.

The stronger summer winds increased the ice–ocean heat exchange, resulting in more summer melting of the simulated sea ice although it should be noted that this effect is weaker than the wind forced differences in winter freezing suggesting the dominance of the mechanical forcing on the summer ice extent differences. The stronger winter winds increased the heat exchange out of the ocean to the atmosphere leading to increased winter freezing, brine rejection, and mixed layer deepening. Stronger northerly or westerly winds that push the ice closer to the coast can also result in more thermodynamic ice creation over the continental shelf in winter by increasing the area subject to large heat losses with little insulating ice cover (Holland et al. 2010). Thus, model overestimates of basal freeze and vertical mixing due to difficulties in compacting the heavy sea ice along the coast with stronger winds (too much heat conduction through too thin ice) would be balanced out by an underestimate of vertical mixing because there should be more open areas over the shelf. Holland et al. (2010) maintain that most of the change in the heat content of the CDW on the shelf resulting from changes in the winds is due to brine rejection from sea ice growth, which causes convection that mixes the heat upward. However, for the WAP simulations, brine rejection from increased sea ice formation was not the only cause of the increased flux of heat from the CDW. The stronger brine rejection with increased winds does deepen the mixed layer and thus make it easier for stronger individual high energy surface forcing events to mix heat out of the CDW. However, the flux of heat out of the deeper waters resulting from increased winds differed from that obtained from the base case (Fig. 8), even for times when there was not a significantly stronger flux of mass into the ice (i.e., when there was not a stronger flux of salt into the ocean). Still, the basic conclusion that ice shelves in the Bellingshausen–WAP region are likely to be more affected by changes in local surface conditions than by variability in the flux of CDW onto the continental shelf is supported by this study and that of Holland et al. (2010).

c. Impacts on biological processes

Changes in across-shelf transport of CDW and vertical mixing potentially have important implications for the biological productivity of the WAP continental shelf. CDW intrusions bring nitrate, silicate, and phosphate onto the WAP shelf (Prézelin et al. 2004; Serebrennikova and Fanning 2004), which mix upward into the euphotic zone resulting in increased primary production (Prézelin et al. 2000, 2004). Prézelin et al. (2004) suggested that CDW may also provide a source of the micronutrient iron, which limits phytoplankton growth in many regions of the Antarctic continental shelf (de Baar et al. 1990; Martin et al. 1990; Sedwick and DiTullio 1997; Sedwick et al. 2000; Coale et al. 2003; Bertrand et al. 2007). CDW is thought to have high concentrations of this micronutrient (Sedwick et al. 2011) and may provide a significant iron source to the euphotic zone of the Ross Sea (Hiscock 2004; Peloquin and Smith 2007). Scaling arguments (Dinniman et al. 2011) suggested that input of dissolved iron from CDW into the upper water column may not be significant for the WAP shelf. However, the relative contribution of CDW-derived iron could change with modifications in the across-shelf transport and vertical mixing.

Estimated net annual primary production in the coastal waters on the WAP shelf is 47–351 g(C) m^{-2} yr^{-1} (Ducklow et al. 2006) and integrated shelf productivity is approximately 60 g(C) m^{-2} yr^{-1} (Smith and Comiso 2008). Thus, our estimates [up to 10 g(C) m^{-2} yr^{-1}] show that CDW-derived iron may not provide a significant enhancement to biological productivity of the WAP continental shelf. However, the estimates of productivity that can be supported increased with stronger winds (Table 4). An increase of just 20% in the wind strength could provide sufficient iron to have a noticeable impact on primary production. However, the corresponding increased vertical mixing would also increase the summer mixed layer depth and potentially reduce primary production. Increased winds have been measured over the past two decades on the southern portions of the WAP shelf, but have been accompanied

by increases in primary productivity, which may be attributed to decreased sea ice concentration and increased light availability (Montes-Hugo et al. 2009).

5. Summary

Changes in the physical environment of the Antarctic Peninsula region and the thermohaline properties of Southern Ocean water masses that could affect CDW transport and ice shelf basal melt are already underway. There are indications that the temperature of UCDW has increased, at least in some areas (Jacobs et al. 2002; Aoki et al. 2005). Atmospheric temperature over the Antarctic Peninsula has increased (Vaughan et al. 2003; Turner et al. 2005) as have the strength of the westerlies (Marshall et al. 2006) and the frequency of mesoscale cyclones (Lubin et al. 2008). The decrease in yearly sea ice duration and monthly sea ice concentration in the Bellingshausen Sea and Antarctic Peninsula region has been rapid and the most pronounced of any area of the Antarctic (Smith and Stammerjohn 2001; Stammerjohn et al. 2008b).

The WAP simulations showed that strengthening of the winds and the ACC will result in more CDW on the WAP continental shelf, enhanced provisioning of heat to the upper-shelf waters, and reduction in sea ice extent. The consequences of these changes for the WAP ice shelves seem to differ depending on the ice shelf draft and connection to the adjacent coastal ocean with deeper ice shelves (e.g., GVIIS) generally having less basal melting and shallower ice shelves (e.g., WIS) having more. Either way, the relationship among ice shelf basal melt rate, CDW volume flux, and strengthening polar westerlies is complex. Understanding these interactions requires development of long-term Southern Ocean–observing systems that provide coincident measurements of ocean, atmospheric, and ice shelf conditions. High-resolution coupled models developed for local, regional, and circumpolar scales are then needed to integrate the observations and project future conditions.

Changes in the flux of CDW onto the WAP continental shelf have important implications for the biological productivity of this system. The reduction in winter sea ice that occurs with a 20% increase in winds would potentially affect many components of the local food web, such as Antarctic krill (*Euphausia superba*), that require sea ice as an overwintering habitat. Reduction in the presence and/or productivity of these organisms would alter the productivity and possibly the structure of the local food web. The potential increase in productivity that would accrue from the influx of more dissolved iron in CDW may not be sufficient to offset the decrease resulting from a modified habitat.

REFERENCES

Aoki, S., N. L. Bindoff, and J. A. Church, 2005: Interdecadal water mass changes in the Southern Ocean between 30°E and 160°E. *Geophys. Res. Lett.,* **32,** L07607, doi:10.1029/2004GL022220.

Bertrand, E. M., M. A. Saito, J. M. Rose, C. R. Riesselman, M. C. Lohan, A. E. Noble, P. A. Lee, and G. R. DiTullio, 2007: Vitamin B_{12} and iron colimitation of phytoplankton growth in the Ross Sea. *Limnol. Oceanogr.,* **52,** 1079–1093.

Bolmer, S. T., 2008: A note on the development of the bathymetry of the continental margin west of the Antarctic Peninsula from 65° to 71°S and 65° to 78°W. *Deep-Sea Res. II,* **55,** 271–276, doi:10.1016/j.dsr2.2007.10.004.

Bromwich, D. H., A. J. Monaghan, K. W. Manning, and J. G. Powers, 2005: Real-time forecasting for the Antarctic: An evaluation of the Antarctic Mesoscale Prediction System (AMPS). *Mon. Wea. Rev.,* **133,** 579–603.

Budgell, P., 2005: Numerical simulation of ice-ocean variability in the Barents Sea region towards dynamical downscaling. *Ocean Dyn.,* **55,** 370–387.

Callahan, J. E., 1972: The structure and circulation of deep water in the Antarctic. *Deep-Sea Res.,* **19,** 563–575.

Carton, J. A., and B. A. Giese, 2008: A reanalysis of ocean climate using SODA. *Mon. Wea. Rev.,* **136,** 2999–3017.

Chen, J. L., C. R. Wilson, D. Blakenship, and B. D. Tapley, 2009: Accelerated Antarctic ice loss from satellite gravity measurements. *Nat. Geosci.,* **2,** 859–862, doi:10.1038/ngeo694.

Coale, K. H., X. Wang, S. J. Turner, and K. S. Johnson, 2003: Phytoplankton growth and biological response to iron and zinc addition in the Ross Sea and Antarctic Circumpolar Current along 170°W. *Deep-Sea Res. II,* **50,** 635–653.

Corr, H. F. J., A. Jenkins, K. W. Nicholls, and C. S. M. Doake, 2002: Precise measurement of changes in ice-shelf thickness by phase-sensitive radar to determine basal melt rates. *Geophys. Res. Lett.,* **29,** 1226, doi:10.1029/2001GL014606.

deBaar, H. J. W., A. G. J. Buma, R. F. Nolting, G. C. Cadée, G. Jacques, and P. J. Tréguer, 1990: On iron limitation of the Southern Ocean: Experimental observations in the Weddell and Scotia Sea. *Mar. Ecol. Prog. Ser.,* **65,** 105–122.

Dinniman, M. S., and J. M. Klinck, 2004: A model study of circulation and cross shelf exchange on the west Antarctic Peninsula continental shelf. *Deep-Sea Res. II,* **51,** 2003–2022.

——, ——, and W. O. Smith Jr., 2003: Cross-shelf exchange in a model of the Ross Sea circulation and biogeochemistry. *Deep-Sea Res. II,* **50,** 3103–3120.

——, ——, and ——, 2007: The influence of sea ice cover and icebergs on circulation and water mass formation in a numerical circulation model of the Ross Sea, Antarctica. *J. Geophys. Res.,* **112,** C11013, doi:10.1029/2006JC004036.

——, ——, and ——, 2011: A model study of Circumpolar Deep Water on the west Antarctic Peninsula and Ross Sea continental shelves. *Deep-Sea Res. II,* **58,** 1508–1523, doi:10.1016/j.dsr2.2010.11.013.

Ducklow, H. W., and Coauthors, 2006: Water column processes in the west Antarctic Peninsula and the Ross Sea: Interannual variations and foodweb structure. *Deep-Sea Res. II,* **53,** 834–852.

Fach, B. A., and J. M. Klinck, 2006: Transport of Antarctic krill (*Euphausia superba*) across the Scotia Sea. Part I: Circulation and particle tracking simulations. *Deep-Sea Res. I,* **53,** 987–1010.

Fairall, C. W., E. F. Bradley, J. E. Hare, A. A. Grachev, and J. B. Edson, 2003: Bulk parameterization of air–sea fluxes: Updates and verification for the COARE algorithm. *J. Climate,* **16,** 571–591.

Gnanadesikan, A., and R. W. Hallberg, 2000: On the relationship of the circumpolar current to Southern Hemisphere winds in coarse-resolution ocean models. *J. Phys. Oceanogr.,* **30,** 2013–2034.

Haidvogel, D. B., and Coauthors, 2008: Ocean forecasting in terrain-following coordinates: Formulation and skill assessment of the Regional Ocean Modeling System. *J. Comput. Phys.,* **227,** 3595–3624, doi:10.1016/j.jcp.2007.06.016.

Häkkinen, S., and G. L. Mellor, 1992: Modeling the seasonal variability of a coupled Arctic ice–ocean system. *J. Geophys. Res.,* **97,** 20 285–20 304.

Harangozo, S. A., 2006: Atmospheric circulation impacts on winter maximum sea ice extent in the west Antarctic Peninsula region (1979–2001). *Geophys. Res. Lett.,* **33,** L02502, doi:10.1029/2005GL024978.

Hellmer, H. H., S. S. Jacobs, and A. Jenkins, 1998: Oceanic erosion of a floating Antarctic glacier in the Amundsen Sea. *Ocean, Ice, and Atmosphere: Interactions at the Antarctic Continental Margin,* S. S. Jacobs and R. F. Weiss, Eds., AGU Antarctic Research Series, Vol. 75, American Geophysical Union, 83–99.

Hiscock, M., 2004: The regulation of primary productivity in the Southern Ocean. Ph.D. dissertation, Duke University, 150 pp.

Hofmann, E. E., J. M. Klinck, D. P. Costa, K. L. Daly, J. J. Torres, and W. R. Fraser, 2002: U.S. Southern Ocean global ecosystems dynamics program. *Oceanography,* **15,** 64–74.

Hogg, A. McC., M. P. Meredith, J. R. Blundell, and C. Wilson, 2008: Eddy heat flux in the Southern Ocean: Response to variable wind forcing. *J. Climate,* **21,** 608–620.

Holland, D. M., and A. Jenkins, 1999: Modeling thermodynamic ice–ocean interactions at the base of an ice shelf. *J. Phys. Oceanogr.,* **29,** 1787–1800.

Holland, P. R., A. Jenkins, and D. M. Holland, 2010: Ice and ocean processes in the Bellingshausen Sea, Antarctica. *J. Geophys. Res.,* **115,** C05020, doi:10.1029/2008JC005219.

Howard, S. L., J. Hyatt, and L. Padman, 2004: Mixing in the pycnocline over the western Antarctic Peninsula shelf during Southern Ocean GLOBEC. *Deep-Sea Res. II,* **51,** 1965–1979.

Humbert, A., D. Gross, R. Müller, M. Braun, R. S. W. van de Wal, M. R. van den Broeke, D. G. Vaughan, and W. J. van de Berg, 2010: Deformation and failure of the ice bridge on Wilkins Ice Shelf, Antarctica. *Ann. Glaciol.,* **51,** 49–55.

Hunke, E. C., 2001: Viscous-plastic sea ice dynamics with the EVP model: Linearization issues. *J. Comput. Phys.,* **170,** 18–38.

——, and J. K. Dukowicz, 1997: An elastic–viscous–plastic model for sea ice dynamics. *J. Phys. Oceanogr.,* **27,** 1849–1867.

Jacobs, S. S., 2006: Observations of change in the Southern Ocean. *Philos. Trans. Roy. Soc.,* **A364,** 1657–1684, doi:10.1098/rsta.2006.1794.

——, H. H. Hellmer, and A. Jenkins, 1996: Antarctic ice sheet melting in the Southeast Pacific. *Geophys. Res. Lett.,* **23,** 957–960.

——, C. F. Giulivi, and P. A. Mele, 2002: Freshening of the Ross Sea during the late 20th century. *Science,* **297,** 386–389, doi:10.1126/science.1069574.

Jenkins, A., and S. S. Jacobs, 2008: Circulation and melting beneath George VI Ice Shelf, Antarctica. *J. Geophys. Res.,* **113,** C04013, doi:10.1029/2007JC004449.

——, D. G. Vaughan, S. S. Jacobs, H. H. Hellmer, and J. R. Keys, 1997: Glaciological and oceanographic evidence of high melt rates beneath Pine Island Glacier, West Antarctica. *J. Glaciol.,* **43,** 114–121.

Klinck, J. M., 1998: Heat and salt changes on the continental shelf west of the Antarctic Peninsula between January 1993 and January 1994. *J. Geophys. Res.,* **103C,** 7617–7636.

——, E. E. Hofmann, R. C. Beardsley, B. Salihoglu, and S. Howard, 2004: Water-mass properties and circulation on the west Antarctic Peninsula Continental Shelf in austral fall and winter 2001. *Deep-Sea Res. II,* **51,** 1925–1946.

Kwok, R., and J. C. Comiso, 2002: Spatial patterns of variability in Antarctic surface temperature: Connections to the Southern Hemisphere Annular Mode and the Southern Oscillation. *Geophys. Res. Lett.,* **29,** 1705, doi:10.1029/2002GL015415.

Large, W. G., J. C. McWilliams, and S. C. Doney, 1994: Oceanic vertical mixing: A review and a model with nonlocal boundary layer parameterization. *Rev. Geophys.,* **32,** 363–403.

Lefebvre, W., and H. Goosse, 2005: Influence of the Southern Annular Mode on the sea ice-ocean system: The role of the thermal and mechanical forcing. *Ocean Sci.,* **1,** 145–157.

——, ——, R. Timmermann, and T. Fichefet, 2004: Influence of the Southern Annular Mode on the sea ice–ocean system. *J. Geophys. Res.,* **109,** C09005, doi:10.1029/2004JC002403.

Liu, J., J. A. Curry, and D. G. Martinson, 2004: Interpretation of recent Antarctic sea ice variability. *Geophys. Res. Lett.,* **31,** L02205, doi:10.1029/2003GL018732.

Lubin, D., R. A. Wittenmyer, D. H. Bromwich, and G. J. Marshall, 2008: Antarctic Peninsula mesoscale cyclone variability and climatic impacts influenced by the SAM. *Geophys. Res. Lett.,* **35,** L02808, doi:10.1029/2007GL032170.

Lythe, M. B., and Coauthors, 2001: BEDMAP: A new ice thickness and subglacial topographic model of Antarctica. *J. Geophys. Res.,* **106B,** 11 335–11 351.

Makinson, K., M. Schröder, and S. Østerhus, 2006: Effect of critical latitude and seasonal stratification on tidal current profiles along Ronne Ice Front, Antarctica. *J. Geophys. Res.,* **111,** C03022, doi:10.1029/2005JC003062.

Marshall, G. J., 2003: Trends in the Southern Annular Mode from observations and reanalyses. *J. Climate,* **16,** 4134–4143.

——, A. Orr, N. P. M. van Lipzig, and J. C. King, 2006: The impact of a changing Southern Hemisphere Annular Mode on Antarctic Peninsula summer temperatures. *J. Climate,* **19,** 5388–5404.

Martin, J. H., S. E. Fitzwater, and R. M. Gordon, 1990: Iron deficiency limits plankton growth in Antarctic waters. *Global Biogeochem. Cycles,* **4,** 5–12.

Martinsen, E. H., and H. Engedahl, 1987: Implementation and testing of a lateral boundary scheme as an open boundary condition in a barotropic ocean model. *Coastal Eng.,* **11,** 603–627.

Martinson, D. G., S. E. Stammerjohn, R. A. Iannuzzi, R. C. Smith, and M. Vernet, 2008: Western Antarctic Peninsula physical oceanography and spatiotemporal variability. *Deep-Sea Res. II,* **55,** 1964–1987.

Maslanyj, M. P., 1987: Seismic bedrock depth measurements and the origin of George VI Sound, Antarctic Peninsula. *British Antarctic Survey Bulletin,* No. 75, British Antarctic Survey, Cambridge, United Kingdom, 51—65.

Massom, R. A., and Coauthors, 2006: Extreme anomalous atmospheric circulation in the west Antarctic Peninsula region in

austral spring and summer 2001/02, and its profound impact on sea ice and biota. *J. Climate,* **19,** 3544–3571.

——, S. E. Stammerjohn, W. Lefebvre, S. A. Harangozo, N. Adams, T. A. Scambos, M. J. Pook, and C. Fowler, 2008: West Antarctic Peninsula sea ice in 2005: Extreme ice compaction and ice edge retreat due to strong anomaly with respect to climate. *J. Geophys. Res.,* **113,** C02S20, doi:10.1029/2007JC004239.

Mellor, G. L., and T. Yamada, 1982: Development of a turbulence closure model for geophysical fluid problems. *Rev. Geophys. Space Phys.,* **20,** 851–875.

——, and L. Kantha, 1989: An ice–ocean coupled model. *J. Geophys. Res.,* **94,** 10 937–10 954.

Meredith, M. P., and A. M. Hogg, 2006: Circumpolar response of Southern Ocean eddy activity to a change in Southern Annular Mode. *Geophys. Res. Lett.,* **33,** L16608, doi:10.1029/2006GL026499.

Miller, R. L., G. A. Schmidt, and D. T. Shindell, 2006: Forced annular variations in the 20th century Intergovernmental Panel on Climate Change Fourth Assessment Report models. *J. Geophys. Res.,* **111,** D18101, doi:10.1029/2005JD006323.

Milliff, R. F., J. Morzel, D. B. Chelton, and M. H. Freilich, 2004: Wind stress curl and wind stress divergence biases from rain effects on QSCAT surface wind retrievals. *J. Atmos. Oceanic Technol.,* **21,** 1216–1231.

Moffat, C., B. Owens, and R. C. Beardsley, 2009: On the characteristics of Circumpolar Deep Water Intrusions to the west Antarctic Peninsula Continental Shelf. *J. Geophys. Res.,* **114,** C05017, doi:10.1029/2008JC004955.

Montes-Hugo, M., S. C. Doney, H. W. Ducklow, W. Fraser, D. Martinson, S. E. Stammerjohn, and O. Schofield, 2009: Recent changes in phytoplankton communities associated with rapid regional climate change along the western Antarctic Peninsula. *Science,* **323,** 1470–1473, doi:10.1126/science.1164533.

Niiler, P. P., and E. B. Kraus, 1977: One-dimensional models of the upper ocean. *Modeling and Prediction of the Upper Layers of the Ocean,* E. B. Krauss, Ed., Pergamon, 143–172.

Olbers, D., D. Borowski, C. Völker, and J.-O. Wölff, 2004: The dynamical balance, transport and circulation of the Antarctic Circumpolar Current. *Antarct. Sci.,* **16,** 439–470, doi:10.1017/S0954102004002251.

Orsi, A. H., T. Whitworth III, and W. D. Nowlin Jr., 1995: On the meridional extent and fronts of the Antarctic Circumpolar Current. *Deep-Sea Res. I,* **42,** 641–673.

Padman, L., D. P. Costa, S. T. Bolmer, M. E. Goebel, L. A. Huckstadt, A. Jenkins, B. I. McDonald, and D. R. Shoosmith, 2010: Seals map bathymetry of the Antarctic continental shelf. *Geophys. Res. Lett.,* **37,** L21601, doi:10.1029/2010GL044921.

——, and Coauthors, 2012: Oceanic controls on mass balance of Wilkins Ice Shelf, Antarctica. *J. Geophys. Res.,* **117,** C01010, doi:10.1029/2011JC007301.

Payne, A. J., A. Vieli, A. Shepherd, D. J. Wingham, and E. Rignot, 2004: Recent dramatic thinning of largest west Antarctic ice stream triggered by oceans. *Geophys. Res. Lett.,* **31,** L23401, doi:10.1029/2004GL021284.

Peloquin, J. A., and W. O. Smith Jr., 2007: Phytoplankton blooms in the Ross Sea, Antarctica: Interannual varaiblility in magnitude, temporal patterns, and composition. *J. Geophys. Res.,* **112,** C08013, doi:10.1029/2006JC003816.

Perlwitz, J., S. Pawson, R. L. Fogt, J. E. Nielsen, and W. D. Neff, 2008: Impact of stratospheric ozone hole recovery on Antarctic climate. *Geophys. Res. Lett.,* **35,** L08714, doi:10.1029/2008GL033317.

Potter, J. R., and J. G. Paren, 1985: Interaction between ice shelf and ocean in George VI Sound, Antarctica. *Oceanology of the Antarctic Continental Shelf,* S. S. Jacobs, Ed., AGU Antarctic Research Series, Vol. 43, American Geophysical Union, 35–58.

Powers, J. G., A. J. Monaghan, A. M. Cayette, D. H. Bromwich, Y.-H. Kuo, and K. W. Manning, 2003: Real-time mesoscale modeling over Antarctica: The Antarctic Mesoscale Prediction System (AMPS). *Bull. Amer. Meteor. Soc.,* **84,** 1533–1545.

Prézelin, B. B., E. E. Hofmann, C. Mengelt, and J. M. Klinck, 2000: The linkage between Upper Circumpolar Deep Water (UCDW) and phytoplankton assemblages on the west Antarctic Peninsula continental shelf. *J. Mar. Res.,* **58,** 165–202.

——, ——, M. Moline, and J. M. Klinck, 2004: Physical forcing of phytoplankton community structure and primary production in continental shelf waters of the western Antarctic Peninsula. *J. Mar. Res.,* **62,** 419–460.

Pritchard, H. D., R. J. Arthern, D. G. Vaughan, and L. A. Edwards, 2009: Extensive dynamic thinning on the margins of the Greenland and Antarctic ice sheets. *Nature,* **461,** 971–975, doi:10.1038/nature08471.

Read, J. F., R. T. Pollard, A. I. Morrison, and C. Symon, 1995: On the southerly extent of the Antarctic Circumpolar Current in the southeast Pacific. *Deep-Sea Res. II,* **42,** 933–954.

Rignot, E., J. L. Bamber, M. R. van den Broeke, C. Davis, Y. Li, W. van de Berg, and E. van Meijgaard, 2008: Recent Antarctic ice mass loss from radar interferometry and regional climate modeling. *Nat. Geosci.,* **1,** 106–110, doi:10.1038/ngeo102.

Scambos, T., H. A. Fricker, C.-C. Liu, J. Bohlander, J. Fastook, A. Sargent, R. Massom, and A.-M. Wu, 2009: Ice shelf disintegration by plate bending and hydrofracture: Satellite observations and model results of the 2008 Wilkins Ice Shelf break-up. *Earth Planet. Sci. Lett.,* **280,** 51–60, doi:10.1016/j.epsl.2008.12.027.

Sedwick, P. N., and G. R. DiTullio, 1997: Regulation of algal blooms in Antarctic shelf waters by the release of iron from melting sea ice. *Geophys. Res. Lett.,* **24,** 2515–2518.

——, ——, and D. J. Mackey, 2000: Iron and manganese in the Ross Sea, Antarctica: Seasonal iron limitation in Antarctic shelf waters. *J. Geophys. Res.,* **105C,** 11 321–11 336.

——, and Coauthors, 2011: Early-season depletion of dissolved iron in the Ross Sea polynya: Implications for iron dynamics on the Antarctic continental shelf. *J. Geophys. Res.,* **116,** C12019, doi:10.1029/2010JC006553.

Sen Gupta, A., and M. H. England, 2006: Coupled ocean–atmosphere–ice response to variations in the Southern Annular Mode. *J. Climate,* **19,** 4457–4486.

Serebrennikova, Y. M., and K. A. Fanning, 2004: Nutrients in the Southern Ocean GLOBEC region: Variations, water circulation, and cycling. *Deep-Sea Res. II,* **51,** 1981–2002.

Shchepetkin, A. F., and J. C. McWilliams, 2009: Correction and commentary for "Ocean forecasting in terrain-following coordinate: Formulation and skill assessment of the regional ocean modeling system" by Haidvogel et al., J. Comp. Phys. 227, pp. 3595–3634. *J. Comput. Phys.,* **228,** 8985–9000, doi:10.1016/j.jcp.2009.09.002.

Shepherd, A., D. J. Wingham, and J. A. D. Mansley, 2002: Inland thinning of the Amundsen Sea sector, West Antarctica. *Geophys. Res. Lett.,* **29,** 1364, doi:10.1029/2001GL014183.

Shindell, D. T., and G. A. Schmidt, 2004: Southern Hemisphere climate response to ozone changes and greenhouse gas increases. *Geophys. Res. Lett.,* **31,** L18209, doi:10.1029/2004GL020724.

Sievers, H., and W. Nowlin, 1984: The stratification and water masses at Drake Passage. *J. Geophys. Res.,* **89C,** 10 489–10 514.

Smith, D. A., and J. M. Klinck, 2002: Water properties on the west Antarctic Peninsula continental shelf: A model study of effects of surface fluxes and sea ice. *Deep-Sea Res. II,* **49,** 4863–4886.

Smith, R. C., and S. E. Stammerjohn, 2001: Variations of surface air temperature and sea ice extent in the western Antarctic Peninsula (WAP) region. *Ann. Glaciol.,* **33,** 493–500.

Smith, W. H., and D. T. Sandwell, 1997: Global sea floor topography from satellite altimetry and ship depth soundings. *Science,* **277,** 1956–1962.

Smith, W. O., Jr., and J. C. Comiso, 2008: Influence of sea ice on primary production in the Southern Ocean: A satellite perspective. *J. Geophys. Res.,* **113,** C05S93, doi:10.1029/2007JC004251.

Son, S.-W., and Coauthors, 2008: The impact of stratospheric ozone recovery on the Southern Hemisphere Westerly Jet. *Science,* **320,** 1486–1489.

Stammerjohn, S. E., D. G. Martinson, R. C. Smith, and R. A. Iannuzzi, 2008a: Sea ice in the western Antarctic Peninsula region: Spatio-temporal variability from ecological and climate change perspectives. *Deep-Sea Res. II,* **55,** 2041–2058.

——, ——, ——, X. Yuan, and D. Rind, 2008b: Trends in Antarctic annual sea ice retreat and advance and their relation to El Niño–Southern Oscillation and Southern Annular Mode variability. *J. Geophys. Res.,* **113,** C03S90, doi:10.1029/2007JC004269.

Steele, M., G. L. Mellor, and M. G. McPhee, 1989: Role of the molecular sublayer in the melting or freezing of sea ice. *J. Phys. Oceanogr.,* **55,** 139–147.

Tagliabue, A., and K. R. Arrigo, 2005: Iron in the Ross Sea: 1. Impact on CO_2 fluxes via variation in phytoplankton functional group and non-Redfield stoichiometry. *J. Geophys. Res.,* **110,** C03009, doi:10.1029/2004JC002531.

Talbot, M. H., 1988: Oceanic environment of George VI Ice Shelf, Antarctic Peninsula. *Ann. Glaciol.,* **11,** 161–164.

Thoma, M., A. Jenkins, D. Holland, and S. Jacobs, 2008: Modelling Circumpolar Deep Water intrusions on the Amundsen Sea continental shelf. *Geophys. Res. Lett.,* **35,** L18602, doi:10.1029/2008GL034939.

Thomas, R., and Coauthors, 2004: Accelerated sea-level rise from West Antarctica. *Science,* **306,** 255–258, doi:10.1126/science.1099650.

Thompson, D. W. J., and J. M. Wallace, 2000: Annular modes in the extratropical circulation. Part I: Month-to-month variability. *J. Climate,* **13,** 1000–1016.

——, and S. Solomon, 2002: Interpretation of recent Southern Hemisphere climate change. *Science,* **296,** 895–899.

Timmermann, R., and A. Beckmann, 2004: Parameterization of vertical mixing in the Weddell Sea. *Ocean Modell.,* **6,** 83–100.

Turner, J., and Coauthors, 2005: Antarctic climate change during the last 50 years. *Int. J. Climatol.,* **25,** 279–294.

Van den Broeke, M. R., and N. P. M. van Lipzig, 2003: Response of wintertime Antarctic temperatures to the Antarctic Oscillation: Results of a regional climate model. *Antarctic Peninsula Climate Variability,* E. Domack, Ed., AGU Antarctic Research Series, Vol. 79, American Geophysical Union, 43–58.

Vaughan, D. G., and Coauthors, 2003: Recent rapid regional climate warming on the Antarctic Peninsula. *Climatic Change,* **60,** 243–274.

Wåhlin, A. K., X. Yuan, G. Björk, and C. Nohr, 2010: Inflow of warm Circumpolar Deep Water in the central Amundsen shelf. *J. Phys. Oceanogr.,* **40,** 1427–1434.

Walker, D. P., M. A. Brandon, A. Jenkins, J. T. Allen, J. A. Dowdeswell, and J. Evans, 2007: Oceanic heat transport onto the Amundsen Sea shelf through a submarine glacial trough. *Geophys. Res. Lett.,* **34,** L02602, doi:10.1029/2006GL028154.

Whitworth, T., III, and W. D. Nowlin Jr., 1987: Water masses and currents of the Southern Ocean at the Greenwich Meridian. *J. Geophys. Res.,* **41,** 629–641.

Willmott, C. J., 1981: On the validation of models. *Phys. Geogr.,* **2,** 184–194.

Zwally, H. J., J. C. Comiso, C. L. Parkinson, D. J. Cavalieri, and P. Gloersen, 2002: Variability of Antarctic sea ice 1979–1998. *J. Geophys. Res.,* **107,** 3041, doi:10.1029/2000JC000733.